



Gain of function due to increased opening probability by two *KCNQ5* pore variants causing developmental and epileptic encephalopathy

Mario Nappi^a, Vincenzo Barrese^a, Lidia Carotenuto^a, Gaetan Lesca^b, Audrey Labalme^b, Dorothee Ville^c, Thomas Smol^d, Mélanie Rama^d, Anne Dieux-Coeslier^e, Clotilde Rivier-Ringenbach^f, Maria Virginia Soldovieri^g, Paolo Ambrosino^h, Ilaria Mosca^g, Michael Puschⁱ, Francesco Miceli^{a,1}, and Maurizio Tagliatela^{a,1,2}

Edited by Lily Jan, HHMI, University of California, San Francisco, CA; received September 16, 2021; accepted January 27, 2022

Developmental and epileptic encephalopathies (DEEs) are neurodevelopmental diseases characterized by refractory epilepsy, distinct electroencephalographic and neuroradiological features, and various degrees of developmental delay. Mutations in *KCNQ2*, *KCNQ3*, and, more rarely, *KCNQ5* genes encoding voltage-gated potassium channel subunits variably contributing to excitability control of specific neuronal populations at distinct developmental stages have been associated to DEEs. In the present work, the clinical features of two DEE patients carrying de novo *KCNQ5* variants affecting the same residue in the pore region of the Kv7.5 subunit (G347S/A) are described. The *in vitro* functional properties of channels incorporating these variants were investigated with electrophysiological and biochemical techniques to highlight pathophysiological disease mechanisms. Currents carried by Kv7.5 G347 S/A channels displayed: 1) large (>10 times) increases in maximal current density, 2) the occurrence of a voltage-independent component, 3) slower deactivation kinetics, and 4) hyperpolarization shift in activation. All these functional features are consistent with a gain-of-function (GoF) pathogenetic mechanism. Similar functional changes were also observed when the same variants were introduced at the corresponding position in Kv7.2 subunits. Nonstationary noise analysis revealed that GoF effects observed for both Kv7.2 and Kv7.5 variants were mainly attributable to an increase in single-channel open probability, without changes in membrane abundance or single-channel conductance. The mutation-induced increase in channel opening probability was insensitive to manipulation of membrane levels of the critical Kv7 channel regulator PIP₂. These results reveal a pathophysiological mechanism for *KCNQ5*-related DEEs, which might be exploited to implement personalized treatments.

potassium channels | developmental and epileptic encephalopathies | genotype–phenotype correlations

Epilepsy is a chronic neurological disorder characterized by a propensity to recurrent unprovoked seizures. In the last 2 decades, a genetic etiology has been revealed in more than half of epilepsies (1). Variants in the genes encoding potassium (K⁺) channel subunits regulating intrinsic electrical properties and response to synaptic inputs in neuronal cells are frequent causes of genetic epilepsies. Among them, mutations in *KCNQ2* and *KCNQ3* genes are known to cause epileptic phenotypes with markedly heterogeneous clinical features ranging from self-limiting, drug-responsive forms to severe developmental and epileptic encephalopathies (DEEs) characterized by drug-resistant seizures, distinct electroencephalographic (EEG) and neuroradiological features, and various degrees of neurodevelopmental delay (2, 3). By contrast, variants in *KCNQ5* (4, 5) have been only recently identified in patients with intellectual disability (ID) or DEEs (6). While several hundred disease-causing variants are known in *KCNQ2* and a few tens in *KCNQ3*, only five *KCNQ5* de novo heterozygous variants are currently known to be associated with distinct human phenotypes. In particular, four patients with ID with or without seizures carried *KCNQ5* missense mutations (6), whereas another patient affected by mild ID with history of absence epilepsy in adolescence and no EEG nor MRI alterations carried an intragenic duplication of the *KCNQ5* gene in heterozygosity (7).

Kv7.2, Kv7.3, and Kv7.5 subunits, encoded by *KCNQ2*, *KCNQ3*, and *KCNQ5* genes, respectively, contribute to the molecular heterogeneity of the M current (I_{KM}), a critical regulator of neuronal excitability (3–5). Kv7.5 subunits also provide an essential component of the medium and, possibly, slow after hyperpolarization (m_{AHP}, s_{AHP}) currents which activate after a train of action potentials (8). This contribution appears to be highly neuronal population specific, being more prominent in CA3 where Kv7.5

Significance

Variants in genes encoding neuronally expressed potassium channel subunits are frequent causes of developmental and epileptic encephalopathies (DEEs). Characterization of their functional consequences is critical to confirm diagnosis, assess prognosis, and implement personalized treatments. In the present work, we describe two patients carrying variants in *KCNQ5*, a gene very recently and rarely found involved in DEEs, and reveal that they both cause remarkable gain-of-function consequences on channel activity. A PIP₂-independent increase in open probability, without effects on membrane abundance or single-channel conductance, was responsible for the observed mutation-induced functional changes, thus revealing a pathomolecular disease mechanism for DEEs.

Author contributions: G.L., M.P., F.M., and M.T. designed research; M.N., V.B., L.C., G.L., A.L., D.V., T.S., M.R., A.D.-C., C.R.-R., M.V.S., P.A., I.M., M.P., F.M., and M.T. performed research; M.N., V.B., L.C., G.L., A.L., D.V., T.S., M.R., A.D.-C., C.R.-R., M.V.S., P.A., I.M., M.P., F.M., and M.T. analyzed data; and V.B., F.M., and M.T. wrote the paper.

The authors declare no competing interest.

This article is a PNAS Direct Submission.

Copyright © 2022 the Author(s). Published by PNAS. This article is distributed under Creative Commons Attribution-NonCommercial-NoDerivatives License 4.0 (CC BY-NC-ND).

¹F.M. and M.T. contributed equally to this work.

²To whom correspondence may be addressed. Email: mtagliat@unina.it.

This article contains supporting information online at <http://www.pnas.org/lookup/suppl/doi:10.1073/pnas.2116887119/-DCSupplemental>.

Published April 4, 2022.

subunits modulate synaptic inhibition and shape hippocampal network synchronization (9). Despite such functional evidence, the definition of a more precise pathophysiological role for Kv7.5 in human epileptic and/or developmental diseases is precluded by the lack of pharmacological tools specifically targeting Kv7.5 subunits (10) and by the potential confounder represented by compensatory mechanisms in other KCNQ genes in genetically engineered mice (11). Thus, the identification of individuals with distinct clinical phenotypes caused by pathogenic variants in *KCNQ5* is critical to unravel the contribution of this gene in human pathophysiology and to highlight clinical differences among *KCNQ2*-, *KCNQ3*-, and *KCNQ5*-related disorders. Moreover, functional characterization of the disease-causing variants is required to confirm pathogenicity, identify pathogenic mechanisms, and hypothesize personalized treatments reversing the underlying pathology.

In the present work, we report the detailed clinical and genetic characteristics of two patients with DEE or ID without seizures each carrying a de novo heterozygous variant (G347S and G347A) affecting the same critical residue in the pore region of Kv7.5. Functional and biochemical analysis *in vitro* revealed that both variants led to remarkable gain-of-function (GoF) effects mainly attributable to a large increase in single-channel open probability, without major changes in membrane subunit abundance or single-channel conductance. Similar functional effects, which were largely insensitive to changes in membrane abundance of phosphatidylinositol 4,5-bisphosphate (PIP₂), a critical regulator of Kv7 channel opening (3), were also observed upon incorporation of the same variant at the corresponding position in Kv7.2 subunits (G313S), highlighting this residue as a key determinant of channel function in Kv7 channels.

Results

Clinical and Genetic Features of the Patients.

Patient 1. This 10-y-old boy is the first child of unrelated parents of French origin. He was born at 37 wk of pregnancy +5 d, with normal neonatal measures. He had a plagiocephaly. Since the first months of life, he had global hypotonia. Sitting position was acquired at 1 y. At 15 mo of life, he experienced several clusters of focal seizures with hypertonia of the left upper arm or of the four limbs, left deviation of the head, staring, and short loss of consciousness. Seizures were not induced by fever. Neurological examination was normal except for the global, previously known, hypotonia but with no psychomotor regression. Interictal EEG recording showed background slowing with diffuse spike waves and diphasic spikes. During drowsiness, high-amplitude spikes became multifocal. He was treated with valproate and clobazam. Brain MRI showed white matter thinning and a voluminous left temporal arachnoid cyst. Video-EEG recording showed sparse left centrotemporal spikes. A seizure was recorded, consisting of bilateral arm extension with predominance on the right side, associated with fast rhythms in the left central parietal region and with postictal slowing in the same region. The patient was operated by kystoperitoneal derivation. Seizure frequency remained variable, up to several episodes in the same day and with periods of 2 wk without seizures. Valproate was sequentially associated with other drugs (levetiracetam, carbamazepine, rufinamide, topiramate, vigabatrin, lamotrigine, and zonisamide) and corticosteroids. The best control was obtained with association of valproate with rufinamide and clonazepam, with multiyear seizure control. At the age of 6, a lymphoblastic leukemia was diagnosed and treated with methotrexate and mercaptopurine.

Currently, the child is still not walking and shows stereotypical movements, no autonomy in everyday life, and very limited language because of a severe ID. Karyotype, array comparative genomic hybridization (Array-CGH), fragile-X expansion study, and metabolic screening including very long-chain fatty acid, thyroid hormones, blood amino acid, urine organic acid, blood lactate and pyruvate, ammoniemia, and Western blotting of the transferrin isoforms were normal.

Trio-based exome sequencing (including DNA from the patient and unaffected parents) showed a de novo heterozygous transition of *KCNQ5*: Chr6(GrCh37):g.73821040G > A, NM_001160133.1:c.1039G > A, predicted to replace a glycine (G) with a serine (S), p.G347S. *In silico* predictions (sorting intolerant from tolerant or SIFT, Polyphen-2, MutationTaster) were in favor of a deleterious effect. The combined annotation dependent depletion (CADD) score was 32. The variant was absent from the Genome Aggregation Database (gnomAD) of control individuals.

Patient 2. The patient is a 15-y-old girl, born to healthy nonrelated parents. She was born at term with normal growth. She walked at 18 mo and had speech delay. At the last referral at 13 y, she had moderate to severe ID. She had mild behavioral issues with autistic features. Height was on -2 SD, weight on -1 SD, and occipitofrontal circumference (OFC) on +0.5 SD. Upon examination, she had a low hanging columella, enlarged naris, and hypertrichosis on the backside and on the arms. She also presented a pyramidal and an extrapyramidal syndrome. Initial head MRI and EEG studies around age 8 y were normal. A panel of 482 genes for neurodevelopmental disorders was performed in trio and showed a de novo heterozygous alteration in *KCNQ5* Chr6(GrCh37):g.73821041G > C NM_001160133.1:c.1040G > C, leading to the substitution of the amino acid glycine with an alanine (A), p.G347A. *In silico* predictions (SIFT, Polyphen-2, MutationTaster) were in favor of a deleterious effect. The CADD score was 26.7. The variant was absent from the gnomAD database of control individuals.

Functional Properties of Kv7.5 G347S (G1S) and G347A (G1A) Subunits When Expressed as Homomers or as Heteromers with Kv7.3 and/or Kv7.5 Subunits. The two *KCNQ5* variants identified in patients 1 and 2 both affect the first glycine (G347) of the -GSG- motif located in the distal end of the S₆ transmembrane segment of Kv7.5 subunits; thus, G347 will be referred to as G1, and variants at this position will be referred to as G1S and G1A (Fig. 1 *A* and *B*). To evaluate the effects of the G1S and G1A variants on Kv7.5 channel function, Kv7.5, Kv7.5 G1S, or Kv7.5 G1A channels were expressed in homomeric configuration in Chinese hamster ovary (CHO) cells. Cells expressing Kv7.5 channels generated small voltage-dependent K⁺-selective currents which activated around -60 mV with a rather slow time course of activation (Fig. 1*C* and Table 1) (12). At the holding voltage of -80 mV, Kv7.5 channels were closed; therefore, the ratio between the currents measured at the beginning of the depolarization step (time indicated by A in Fig. 1*D*) and those at the end of the 0 mV depolarization (time indicated by B in Fig. 1*D*) was close to zero (Table 1).

Replacement of the G1 residue with a serine (Kv7.5 G1S) or an alanine (Kv7.5 G1A) increased by >10-fold the currents carried by Kv7.5 channels (Fig. 1*C* and Table 1). In both G1S or G1A Kv7.5 channels, the activation process was described by two distinct components: an instantaneous voltage-independent one (I_{INST}), accounting for about 45 to 50% of the total current (Table 1), followed by a slower voltage- and time-dependent component (I_{VDEP}). Because of the coexistence of

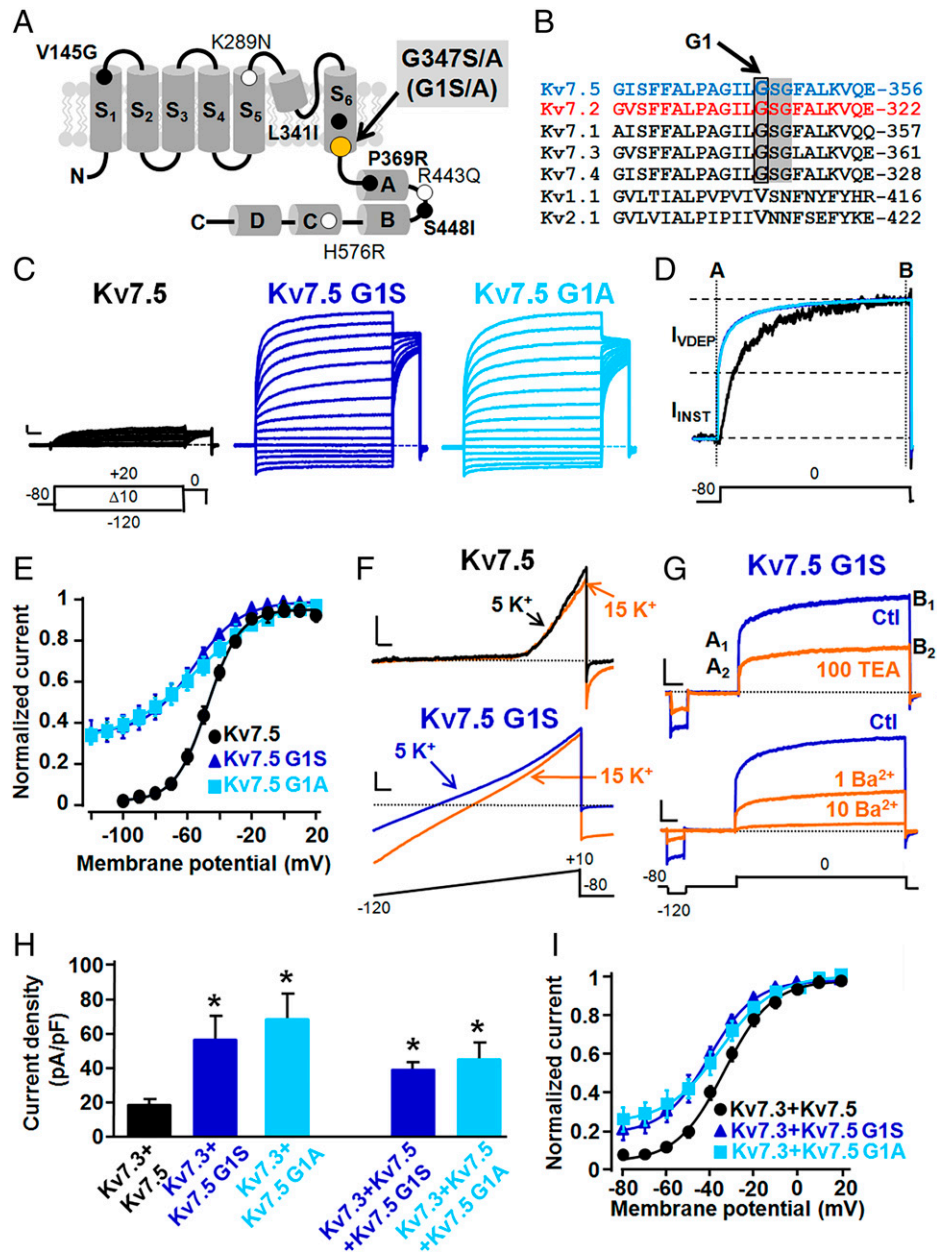


Fig. 1. Topological location of the G347 (G1) residue and functional characterization of Kv7.5, Kv7.5 G1S, and Kv7.5 G1A channels. (A) Schematic representation of a single Kv7.5 subunit, showing the position of the G1 residue herein investigated (gray highlighting) and of the currently known Kv7.5 pathogenic variants whose functional characteristics have been studied (bold characters) or are yet unknown (regular characters). (B) Sequence alignment of the bottom part of the S₆ segments of the indicated Kv subunits (<https://www.ebi.ac.uk/Tools/psa/>). The shaded region highlights the -GSG- motif, with the G1 residue indicated by the box. (C) Macroscopic currents from Kv7.5, Kv7.5 G1S, and Kv7.5 G1A homomeric channels, in response to the indicated voltage protocol. Current scale, 200 pA; time scale, 200 ms. (D) Superimposed normalized current traces from Kv7.5 (black), Kv7.5 G1S (dark blue), and Kv7.5 G1A (light blue) homomeric channels. A and B represent time points at which instantaneous and steady-state currents were measured, respectively; (B - A)/B × 100 represents the fraction of voltage-dependent, time-dependent current (*I*_{VDEP}); and the fraction of voltage-independent, instantaneous current (*I*_{INST}) was calculated as (A/B) × 100 (or 1 - *I*_{VDEP}). (E) Conductance/voltage curves for the indicated channels. Continuous lines are Boltzmann fits of the experimental data. (F) Ramp currents from the indicated channels using the voltage protocol shown at the bottom in 5 and 15 mM extracellular K⁺ ions, as indicated. Current scales, 200 pA for Kv7.5 and 500 pA for Kv7.5 G1S; time scale, 20 ms. (G) Effect of 100 mM TEA_e (Upper) or 1 to 10 mM Ba²⁺_e (Lower) on Kv7.5 G1S currents recorded with the voltage protocol shown at the bottom. A₁ and A₂ indicate the *I*_{INST} current values measured in control and drug-containing solutions, respectively; B₁ and B₂ indicate the steady-state (*I*_{INST} + *I*_{VDEP}) current values measured in control and drug-containing solutions, respectively. Current scales, 200 pA for Upper (100 mM TEA_e) and 500 pA for Lower (1 to 10 mM Ba²⁺_e); time scale, 100 ms. (H) Quantification of current densities recorded from cells transfected with the indicated cDNA constructs. Asterisks indicate values significantly different (**P* < 0.05) from their respective control (Kv7.3 + Kv7.5). (I) Conductance/voltage curves for the currents recorded from cells transfected with the indicated cDNA constructs. Continuous lines are Boltzmann fits of the experimental data.

voltage-independent and voltage-dependent components, even at very hyperpolarized membrane potential values (-120 mV), a significant fraction of Kv7.5 G1S and G1A channels failed to close, leading to the appearance of large inward currents. Boltzmann analysis (Eq. 1 in *Materials and Methods*) showed that the half-activation potential (*V*_{1/2}) of *I*_{VDEP} in Kv7.5 G1S or Kv7.5 G1A channels was hyperpolarized by 13 and 9 mV, respectively

(Fig. 1E and Table 1). When compared to Kv7.5 channels, *I*_{VDEP} carried by Kv7.5 G1S/A channels showed slower deactivation kinetics; indeed, at -120 mV, the deactivation time constants were: 43.0 ± 6.0, 84.9 ± 14.3, or 87.3 ± 9.8 ms, for Kv7.5, Kv7.5 G1S, or Kv7.5 G1A channels, respectively (*P* < 0.05 for both mutants when compared to wild-type Kv7.5 channels). The reversal potential (*V*_{rev}) estimated from tail current

Table 1. Biophysical properties of wild-type and mutant channels investigated

Construct(s)	Amount cDNA (μg)	n	$V_{1/2}$ (mV)	K (mV/e-fold)	I_{INST} at 0 mV (%)	Current density at 0 mV (pA/pF)
Untransfected		5	–	–	–	0.5 ± 0.2
Kv7.5	3	25	-42.0 ± 2.1	10.4 ± 0.9	3 ± 1	11.6 ± 2.0
Kv7.5 G1S	3	14	$-54.8 \pm 2.5^*$	$13.5 \pm 0.5^*$	$45 \pm 4^*$	$176.5 \pm 24.5^*$
Kv7.5 G1A	3	14	$-51.4 \pm 2.0^*$	$18.7 \pm 2.3^*$	$50 \pm 2^*$	$137.6 \pm 27.6^*$
Kv7.5 G1R	3	7	–	–	–	$0.3 \pm 0.1^*$
Kv7.5 G1E	3	7	–	–	–	$0.3 \pm 0.04^*$
Kv7.3	3	9	-37.7 ± 1.1	7.0 ± 0.3	4 ± 2	20.2 ± 2.2
Kv7.3 + Kv7.5	1.5 + 1.5	30	-35.0 ± 0.9	10.2 ± 1.0	8 ± 1	18.8 ± 2.04
Kv7.3 + Kv7.5 G1S	1.5 + 1.5	18	$-42.8 \pm 14.0^\dagger$	11.5 ± 1.4	$19 \pm 4^\dagger$	$57.3 \pm 12.7^\dagger$
Kv7.3 + Kv7.5 G1A	1.5 + 1.5	12	$-39.1 \pm 2.1^\dagger$	15.4 ± 2.4	$24 \pm 3^\dagger$	$85.5 \pm 21.8^\dagger$
Kv7.3 + Kv7.5 + Kv7.5 G1S	1.5 + 0.75 + 0.75	12	-32.3 ± 2.0	$16.7 \pm 1.9^\dagger$	11 ± 3	$45.6 \pm 9.6^\dagger$
Kv7.3 + Kv7.5 + Kv7.5 G1A	1.5 + 0.75 + 0.75	14	-38.0 ± 1.7	10.2 ± 0.7	12 ± 3	$41.9 \pm 7.9^\dagger$
Kv7.2	3	14	-25.6 ± 2.1	12.4 ± 0.8	4 ± 1	31.9 ± 4.0
Kv7.2 G1S	3	9	$-59.9 \pm 4.5^\ddagger$	11.7 ± 0.4	$27 \pm 4^\ddagger$	$215.1 \pm 28.7^\ddagger$
Kv7.2 G1E	3	10	–	–	–	$1.2 \pm 0.3^\ddagger$
Kv7.2 G1R	3	5	–	–	–	$1.2 \pm 0.8^\ddagger$
Kv7.2 + Kv7.2 G1R	1.5 + 1.5	18	-28.0 ± 1.9	10.6 ± 0.8	–	$8.7 \pm 1.3^\ddagger$
Kv7.2 + pcDNA3	0.4 + 1.2	31	-26.8 ± 0.6	10.1 ± 0.5	–	34.8 ± 3.2
Kv7.2 + PIP5K	0.4 + 1.2	24	$-41.8 \pm 0.6^\S$	10.3 ± 0.6	–	$114.6 \pm 8.2^\S$
Kv7.2 G1S + pcDNA3	0.4 + 1.2	8	$-58.0 \pm 0.7^\S$	11.3 ± 0.6	–	$173.8 \pm 32.8^\S$
Kv7.2 G1S + PIP5K	0.4 + 1.2	8	$-76.7 \pm 1.4^\P$	18.8 ± 1.3	–	181.9 ± 27.4

* $P < 0.05$ versus Kv7.5. $^\dagger P < 0.05$ versus Kv7.3 + Kv7.5. $^\ddagger P < 0.05$ versus Kv7.2 (3 μg). $^\S P < 0.05$ versus Kv7.2 + pcDNA3 (0.4 μg + 1.2 μg). $^\P P < 0.05$ versus Kv7.2 G1S + pcDNA3 (0.4 μg + 1.2 μg).

measurements after depolarization to +20 mV for Kv7.5, Kv7.5 G1S, or Kv7.5 G1A channels was -76.2 ± 0.7 , -76.6 ± 0.7 , or -76.7 ± 0.8 mV ($P > 0.05$ for both mutants when compared to wild-type Kv7.5 channels). In Kv7.5 G1S channels, 1.5-s depolarization to +20 mV activates both I_{INST} and I_{VDEP} ; therefore, to characterize the pore properties of I_{INST} in isolation, experiments using fast voltage ramps at hyperpolarized voltages were carried out, as described previously for Kv7.1 channels having similar functional behavior (13). The results obtained revealed that the V_{rev} shifted from -80.7 ± 1.0 to -58.6 ± 1.3 mV when the extracellular solution containing 5 mM K^+ was changed to one containing 15 mM K^+ ($n = 6$; Fig. 1*F*); these values closely resemble those expected from the shift in the Nernst potential for a K^+ -selective current. In addition, I_{INST} and I_{VDEP} showed identical sensitivity to blockade by extracellularly applied tetraethylammonium (TEA_e ; 100 mM) or barium (Ba^{2+}_e ; 1 to 10 mM) ions, two well-known pore blockers of K^+ channels (14, 15); these concentrations were chosen following the results of Schroeder et al. (5), who reported a half-maximal (50%) inhibitory concentration (IC_{50}) for TEA of about ~70 mM and that 1 mM barium blocked about 60% of Kv7.5 currents. At 0 mV, 100 mM TEA_e blocked I_{INST} and I_{VDEP} by 49.3 ± 3.2 and $46.6 \pm 3.3\%$, respectively ($P > 0.05$; $n = 6$). In addition, 1 mM Ba^{2+}_e blocked I_{INST} and I_{VDEP} by 51.0 ± 2.9 and $54.6 \pm 4.6\%$ ($P > 0.05$; $n = 6$), respectively, whereas I_{INST} and I_{VDEP} were blocked by 93.8 ± 1.9 and $89.6 \pm 1.3\%$ ($P > 0.05$; $n = 5$) by 10 mM Ba^{2+}_e . Notably, identical values for blockade by 100 TEA_e , 1 mM Ba^{2+}_e , and 10 mM Ba^{2+}_e were also observed at -120 mV, a membrane potential value where currents were mainly carried by I_{INST} (51.1 ± 3.0 , 59.8 ± 3.2 , and $86.4 \pm 4.5\%$, respectively; $P > 0.05$).

Kv7.5 subunits contribute to neuronal I_{KM} by preferentially forming heteromeric channels with Kv7.3 subunits (4, 5); therefore, experiments were carried out in which complementary DNAs

(cDNAs) encoding Kv7.5 G1S/A subunits were cotransfected with Kv7.3 or Kv7.3 and Kv7.5 cDNAs. When compared to those transfected with Kv7.3 + Kv7.5, CHO cells transfected with Kv7.3 + Kv7.5 G1S and Kv7.3 + Kv7.5 G1A plasmids (1:1 cDNA ratio) showed a threefold increase in maximal current density (Fig. 1*H*), together with the appearance of a nondeactivating, voltage-independent current component, whose size was about 20% at -80 mV (Fig. 1*I*). The depolarization-activated component from cells expressing either G1S or G1A mutant subunits showed a small but statistically significant hyperpolarizing $V_{1/2}$ shift (Table 1). To mimic the genetic balance of the heterozygous individual carrying one mutant *KCNQ5* allele, CHO cells were also transfected with Kv7.3 + Kv7.5 + Kv7.5 G1S or Kv7.3 + Kv7.5 + Kv7.5 G1A at 1:0.5:0.5 cDNA ratio. Under these conditions, a twofold increase in current density from cells expressing Kv7.3 + Kv7.5 + Kv7.5 G1S or Kv7.3 + Kv7.5 + Kv7.5 G1A when compared to those expressing Kv7.3/Kv7.5 was observed. Instead, opposite to what described for Kv7.3 + Kv7.5 G1S- and Kv7.3 + Kv7.5 G1A-transfected cells, no difference in the fraction of I_{INST} or in the $V_{1/2}$ of I_{VDEP} between Kv7.3 + Kv7.5- and Kv7.3 + Kv7.5 + Kv7.5 G1S- or Kv7.3 + Kv7.5 + Kv7.5 G1A-transfected cells could be detected (Table 1).

Functional Analysis of Kv7.2 and Kv7.5 Channels Carrying Naturally and Nonnaturally Occurring Variants at Position G1.

Among voltage-gated K^+ channel subunits, the GSG motif is uniquely present in Kv7s (Fig. 1*B*). In addition to the G1S and G1A in Kv7.5, a G1R variant (substituting the G1 glycine at position 313 with an arginine) has been identified in Kv7.2 in a patient with a severe form of early-onset epileptic encephalopathy (patient 9 in ref. 16). However, no functional data are yet available on Kv7.2 G1R channels. CHO cells expressing Kv7.2 display robust voltage-dependent K^+ currents (Fig. 2*A*) whose activation threshold was more depolarized when compared

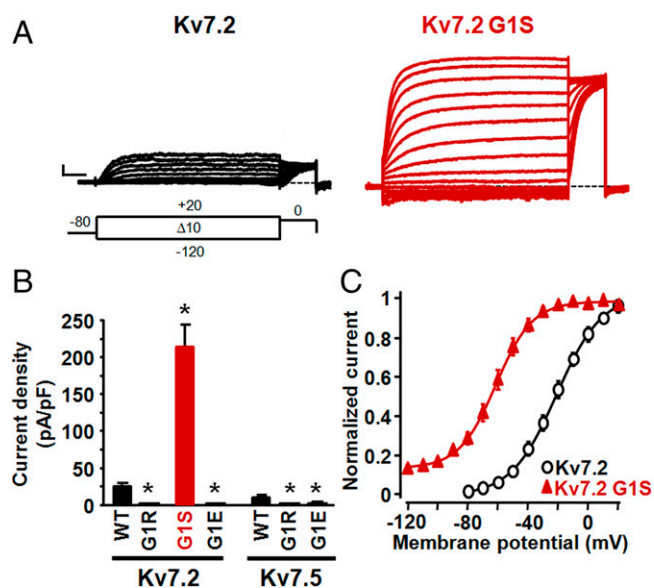


Fig. 2. Functional characterization of Kv7.2 and Kv7.5 channels carrying naturally and nonnaturally occurring variants at position G1. (A) Macroscopic currents from Kv7.2 and Kv7.2 G1S homomeric channels, in response to the indicated voltage protocol. Current scale, 200 pA; time scale, 200 ms. (B) Current densities from the indicated homomeric channels. Asterisks indicate values significantly different ($*P < 0.05$) from respective controls (Kv7.2 or Kv7.5 channels). (C) Conductance/voltage curves for the indicated channels. Continuous lines are Boltzmann fits of the experimental data.

to those of Kv7.3- or Kv7.5-expressing cells, being about -30 mV (Table 1). In contrast, no functional channels could be detected in cells expressing Kv7.2 G1R mutant subunits; current density in Kv7.2 G1R-expressing cells was not different from that of untransfected CHO cells (Table 1). Moreover, coexpression with Kv7.2 G1R subunits (1:1 cDNA transfection ratio) markedly suppressed Kv7.2 currents (Table 1), strongly suggesting that the G1R variant, similarly to most other Kv7.2 variants associated with the classical *KCNQ2*-DEE phenotype (17), caused strong loss-of-function (LoF) effects in vivo, consistent with a dominant-negative pathogenetic disease mechanism (18, 19).

Overall, functional data collected from the analysis of naturally occurring, disease-causing variants suggest that the G1S and G1A substitutions in Kv7.5 caused strong GoF effects, whereas the G1R variant in Kv7.2 determined a marked LoF effect. To investigate whether these strikingly opposite in vitro phenotypes were due to the specific amino acid substitutions at G1 or to the Kv7 subunit in which these were incorporated (Kv7.2 vs. Kv7.5), the G1R variant was introduced in Kv7.5 and the G1S substitution in Kv7.2, thereby swapping the naturally occurring variants between these two channels.

As shown in Fig. 2B, the G1S substitution in Kv7.2 induced a marked increase in current density, together with the appearance of a voltage-independent component (I_{INST} , about 20% of the total current) and a 40-mV leftward shift in the $V_{1/2}$ of the voltage-dependent component (I_{VDEP} ; Fig. 2C and Table 1). On the other hand, the Kv7.5 G1R substitution fully impeded channel function (Fig. 2B and Table 1). These data suggest that in both Kv7.2 and Kv7.5 subunits, qualitatively similar functional consequences were introduced upon substitution of the first G residue within the GSG motif with an S (GoF) or an R (LoF) residue. Similarly to G1R, the G1E substitution also rendered Kv7.5 or Kv7.2 channels nonfunctional (Fig. 2B and Table 1), reinforcing the similarity of the effects of G1 substitutions between Kv7.2 and Kv7.5 channels and suggesting that the unique GoF effect due to the replacement

of the G with a small, polar S residue could not be replicated by incorporation at this position of large and positively or negatively charged side chains such as those provided by R or E residues, respectively.

Molecular Mechanism(s) Underlying the GoF Effects of G1S and G1A Variants. The most striking effect of the G1S/A variants when incorporated in either Kv7.2 or Kv7.5 subunits was a large increase in macroscopic current density, which depends on three parameters: the number of functional channels (N), the single-channel current (i), and the channel opening probability (P_o). Therefore, to investigate variant-induced changes of each of these parameters, we recurred to nonstationary noise analysis (20), given that the small single-channel conductance of Kv7.5 channels (about 2 pS) (21) renders them poorly amenable to direct estimates of these properties using single-channel recordings of unitary events. To perform these experiments, currents from Kv7.5, Kv7.5 G1S, Kv7.2, and Kv7.2 G1S channels expressed in human embryonic kidney-293 (HEK293) cells were activated by 100 depolarizing pulses of 500 ms duration to +20 mV at a frequency of 1 Hz. Potential artifacts due to current rundown ($<20\%$) were minimized by measuring the differences in the current on successive sweeps between consecutive pulses (22). The mean current (top trace), the respective variance (middle trace), and the correlation between the average current and the variance (bottom diagram) for Kv7.5, Kv7.5 G1S, Kv7.2, and Kv7.2 G1S channels are shown in Fig. 3A. Fitting the variance data with Eq. 2 (as described in *Materials and Methods*) failed to reveal difference in the number of functional channels (Fig. 3B) or single-channel current (Fig. 3C) between wild-type Kv7.5 and Kv7.2 channels and their respective G1S mutant counterparts. Instead, a 2.5-/3-fold increase in maximal P_o was observed when the G1S variant was incorporated in Kv7.5 or Kv7.2 channels (Fig. 3D).

It should be underlined that possible errors in N , i , and P_o estimates might occur in nonstationary noise analysis when the variance/mean current plots do not unambiguously show signs of saturation; therefore, in each cell included in the analysis, P_o was also estimated after constraining i by linear fitting of the initial slope of the variance/mean current plots, as previously suggested (23). Using this strategy, P_o values did not vary significantly when compared to those obtained from unconstrained fits. In fact, unconstrained and constrained P_o values were, respectively, 0.25 ± 0.09 and 0.20 ± 0.04 for Kv7.5, 0.63 ± 0.03 and 0.65 ± 0.04 for Kv7.5 G1S, 0.27 ± 0.04 and 0.22 ± 0.04 for Kv7.2, and 0.75 ± 0.05 and 0.77 ± 0.04 for Kv7.2 G1S channels ($P > 0.05$ for each channel type). No changes in N values were also observed when comparing unconstrained and i -constrained fits; these were (in N/pF), respectively, 330 ± 28 and 326 ± 81 for Kv7.5, 371 ± 64 and 362 ± 191 for Kv7.5 G1S, 451 ± 120 and 540 ± 178 for Kv7.2, and 421 ± 222 and 543 ± 178 for Kv7.2 G1S channels ($P > 0.05$ for each channel type). Consistent with these functional results, biochemical experiments revealed no change in Kv7.5 protein levels in total or plasma membrane-purified fractions among Kv7.5-, Kv7.5 G1S-, or Kv7.5 G1A-transfected cells (*SI Appendix, Fig. S1*). Altogether, these data suggest that the G1S substitution, in both Kv7.2 and Kv7.5, caused a strong GoF phenotype by increasing channel opening probability without major changes in the number of functional channels or their unitary conductance.

Effect of the G1S Variant on PIP₂-Dependent Current Regulation. Opening of all Kv7 members requires phosphatidylinositol 4,5-bisphosphate (PIP₂), a membrane lipid which binds to distinct

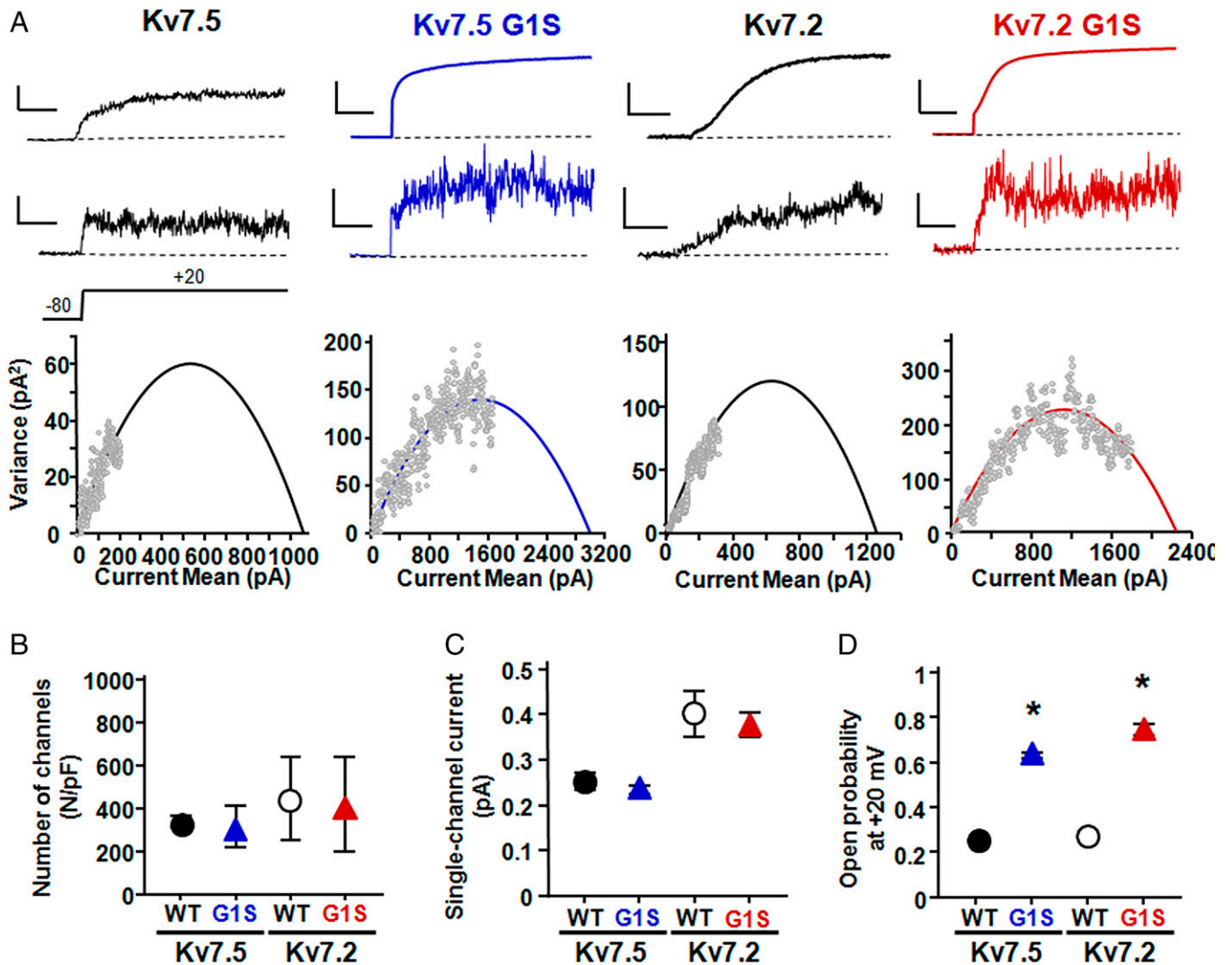


Fig. 3. Nonstationary noise analysis of Kv7.5, Kv7.5 G1S, Kv7.2, and Kv7.2 G1S channels. (A) Representative average response to 100 pulses at +20 mV (Top), of the corresponding variance (Middle), and variance versus current mean plot (Bottom) from Kv7.5, Kv7.5 G1S, Kv7.2, and Kv7.2 G1S channels, as indicated. The continuous lines in Bottom are parabolic fits of the experimental data (Materials and Methods). Current and variance scales are 100 pA and 50 pA² for Kv7.5, 750 pA and 100 pA² for Kv7.5 G1S, 100 pA and 50 pA² for Kv7.2, and 750 pA and 100 pA² for Kv7.2 G1S. Time scale, 100 ms. P_o and I estimates for the four cells shown were 0.18 and 0.20 for Kv7.5, 0.57 and 0.19 for Kv7.5 G1S, 0.25 and 0.38 for Kv7.2, and 0.79 and 0.39 for Kv7.2 G1S. (B–D) Quantification of the number of channels divided by capacitance (B), of the single-channel current (C), and of the opening probability at +20 mV (D). Asterisks indicate values significantly different (*P < 0.05) from respective controls (Kv7.5 channels, Left; Kv7.2 channels, Right).

channel regions at each gating state of the voltage-sensing domain (3, 24). To investigate whether the G1S-induced increase in Kv7.5 P_o was due to an altered channel regulation by PIP₂, resting PIP₂ levels were either decreased by a voltage-sensitive phosphatase from *Danio rerio* (DrVSP), which transiently reduces cellular PIP₂ levels when activated by strong depolarizations (25), or increased by the PIP₂-synthesizing enzyme PIP5K (26). Notably, Kv7.2 rather than Kv7.5 channels were selected for these experiments since they generated larger macroscopic currents when expressed in CHO cells (Table 1). In CHO cells expressing DrVSP, depolarization to +100 mV time-dependently reduced Kv7.2 currents by 60% after 1 s (Fig. 4 A and B); by contrast, currents carried by Kv7.2 G1S channels showed a reduced sensitivity to inhibition upon DrVSP activation at all time points investigated, being inhibited by only 10% of their starting value after 1 s.

On the other hand, increasing cellular PIP₂ levels by PIP5K coexpression caused a threefold enhancement in Kv7.2 peak currents, together with a negative shift in their half-activation potential ($\Delta V_{1/2} = -14.5$ mV), as reported (25–27). When

PIP5K was coexpressed with Kv7.2 G1S channels, no increase in maximal currents occurred, although a leftward shift in activation gating, whose extent was quantitatively similar ($\Delta V_{1/2} = -18.7$ mV) to that observed in Kv7.2 channels, was still observed (Fig. 4 C and D and Table 1).

Discussion

Phenotypic Spectrum and Genotype–Phenotype Correlations in KCNQ5-Related Disorders: Comparison with KCNQ2- and KCNQ3-Related Disorders. *KCNQ2*, *KCNQ3*, and *KCNQ5* genes contribute to the molecular heterogeneity of I_{KM} in specific neuronal subpopulations at distinct developmental periods (3–5, 28). However, while several tens/hundreds of mutations in *KCNQ2* and *KCNQ3* have been identified over 2 decades as responsible for developmental and/or epileptic diseases characterized by a wide spectrum of phenotypic features and severity, only five patients with developmental diseases caused by *KCNQ5* genetic defects have been recently identified. These include four probands who carried heterozygous missense variants: two with mild/

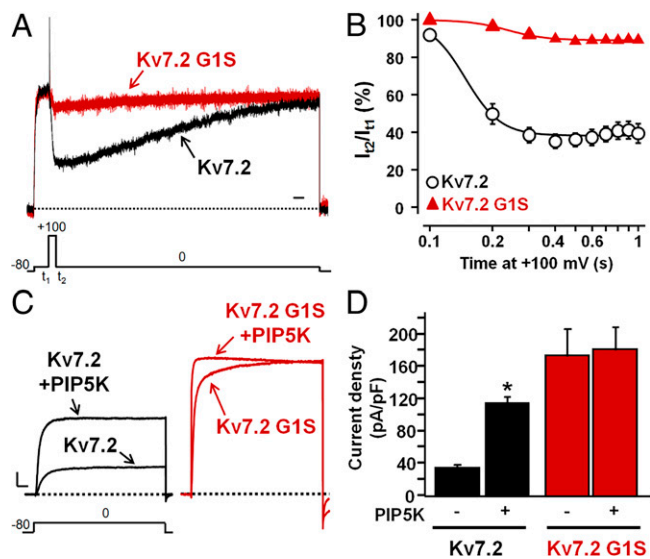


Fig. 4. Effect of DrVSP or PIP5K on Kv7.2 and Kv7.2 G1S homomeric channels. (A) Currents recorded in response to the indicated voltage protocol in cells expressing DrVSP and Kv7.2 or Kv7.2 G1S channels. Time scale, 1 s. (B) Time-dependent current decrease in cells coexpressing the indicated channels and DrVSP, expressed as the ratio between the current values recorded at 0 mV immediately after (t_2) and before (t_1) the Dr-VSP-activating +100 mV depolarizing step. (C) Macroscopic currents recorded in response to the indicated voltage protocol in cells expressing Kv7.2 or Kv7.2 G1S channels in the absence or presence of PIP5K. Current scale, 500 pA; time scale, 200 ms. (D) Current densities at 0 mV from cells expressing Kv7.2 or Kv7.2 G1S channels alone or in combination with PIP5K, as indicated. The asterisk indicates a value significantly different ($*P < 0.05$) from Kv7.2 currents.

moderate ID, limited speech abilities, and no seizures and two with severe–profound ID with seizures and no language (6). Another proband, who carried a heterozygous intragenic duplication of the *KCNQ5* gene, was affected by mild ID with history of absence epilepsy in adolescence and no speech impairment or EEG/MRI alterations (7). These phenotypic characteristics closely resemble those of our two patients, one showing very limited language because of a severe ID and drug-resistant epilepsy (patient 1, G1S) and another suffering from moderate to severe ID without epilepsy (patient 2, G1A). Variants in *KCNQ5* are also emerging in large cohorts of patients with neurodevelopmental disabilities (29, 30); notably, one of these patients carried the same G347S (G1S) variant reported in our patient 1, although no direct phenotype comparison is possible because of the lack of detailed clinical histories in Kaplanis et al. (29). Overall, despite their rarity, *KCNQ5*-related disorders are phenotypically rather different from those caused by pathogenic variants in *KCNQ2* or *KCNQ3* since: 1) no benign (self-limiting) phenotype has yet been described associated to *KCNQ5* variants, while this is quite common for *KCNQ2* and *KCNQ3*; 2) seizures occur in most (but not all) patients with *KCNQ2*- or *KCNQ3*-related disorders, whereas they are not a prominent feature of patients with *KCNQ5* variants; and 3) when present, seizures caused by *KCNQ5* variants occur between 5 mo and 2 y of age, later than those associated to most *KCNQ2* or *KCNQ3* variants, whose first appearance is around 3 d of life. In fact, *KCNQ2* variants account for the largest majority of neonatal-onset genetic epilepsies (31).

Despite these clinical differences, functional analysis in vitro of variants causing *KCNQ2*-, *KCNQ3*-, and *KCNQ5*-related disorders reveal that distinct variants suppress (LoF) or enhance (GoF) channel function. At least for *KCNQ2* and, possibly, *KCNQ3*, a correlation between functional effects in vitro and phenotype has been established (8, 19, 32–35), with strong, dominant-negative LoF variants being responsible for severe

clinical phenotypes and variants found in most self-limiting forms causing haploinsufficiency and milder LoF in vitro effects (28). The severe end of the *KCNQ2*-DEE spectrum is represented by the patient described in Olson et al. (16) who died at 3 mo of age because of a very severe neonatal-onset epileptic encephalopathy and carried a *KCNQ2* variant affecting the G1 residue (G1R); consistent with previously reported data (18, 19), the present functional results reveal strong, dominant-negative LoF effects prompted by the Kv7.2 G1R variant.

Among the four *KCNQ5* pathogenic variants whose functional consequences have been investigated, three (V145G in S₁, L341I in S₆, and S448I in the C-terminal region) decreased, whereas one (P369R; A-helix of the proximal C terminus) enhanced channel function (6). Both G347S/A variants herein described, similarly to the previously described P369R variant, cause GoF effects in vitro; these three GoF variants occur in most severely affected children, with moderate–severe ID and poor or absent verbal abilities and who display severe limb spasticity or are non-ambulatory (6). Such a genotype–phenotype pattern is rather similar to that described for *KCNQ2*, where GoF variants are associated with the most severe phenotype of neonatal-onset encephalopathy with burst-suppression EEG pattern, nonepileptic myoclonus, and poor prognosis with high mortality (34). However, given the rarity of patients with *KCNQ5*-related disorders, neither the functional consequences caused by the mutations nor the variant localization within the channel sequence can fully predict the clinical features of patients carrying *KCNQ5* mutations; thus, no solid genotype–phenotype correlation can be currently drawn. For example, it is yet unclear why patients carrying the G1S or the G1A variants, despite the similarity in their in vitro functional properties, have different epilepsy phenotypes; additional genetic, epigenetic, and epistatic mechanisms likely explain such divergence.

In Vivo Role of Kv7.5 Subunits and Insights into the Phenotypes.

KCNQ5-encoded Kv7.5 subunits preferentially assemble into heteromeric channels with Kv7.3 but not Kv7.2, subunits (5). Whether these heteromeric channels actually exert specific action at selected neuronal sites or just decrease the amount of the more efficient Kv7.2/Kv7.3 channels (5, 36) is still a matter of debate. However, irrespective of the pathophysiological relevance of the Kv7.3/Kv7.5 channels, our functional data seem to suggest that the G1S/A variants in Kv7.5 retain their ability to induce GoF effects even in heteromeric configuration with Kv7.3 subunits, although these effects were quantitatively smaller than those observed for homomeric channels. However, it is difficult to establish the exact channel composition underlying the recorded currents when Kv7.5 G1S/A subunits are coexpressed with Kv7.3 or Kv7.3/Kv7.5 subunits since at variance with Kv7.2 and Kv7.3 (37), currents carried by Kv7.3 and Kv7.5 channels display similar maximal density, gating ($V_{1/2}$), and pharmacological (TEA sensitivity) properties (4, 5).

Within the central nervous system, Kv7.5 expression has been described in cell somata and dendrites in human cortex and hippocampus (38), in glutamatergic synapses of several rat brain stem nuclei (39), and in postsynaptic membrane of mouse vestibular calyx terminals (40). Knock-in mice carrying a Kv7.5 dominant-negative pore variant had normal brain morphology and no seizures but displayed a reduction of the m_{AHP} and s_{AHP} currents in the hippocampus (8). Kv7.5 subunits are highly expressed in the hippocampus (8), where they contribute to shaping sharp waves and ripples activity (41), a highly synchronous population pattern arising from the CA3 region and leading to CA1 fast network oscillation (42). We hypothesize

that the G1S and G1A mutations interfere with the crucial role of Kv7.5 in controlling this pattern of hippocampal excitability which is critically involved in memory consolidation (42), possibly explaining the cognitive changes described in our two patients. On the other hand, it is still unclear how *KCNQ5* GoF changes triggered by the G1S variant lead to cortical hyperexcitability (43). GoF variants occurring in other potassium channel genes have been postulated to decrease interneuron activity and lead to disinhibition; however, animal models more closely reproducing the human pathology are needed to decipher the complex interplay between potassium channels GoF variants and electrical activity during neurodevelopment (2).

Biophysical and Structural Consequences of the G1 Variants.

The functional results obtained suggest that in both Kv7.5 and Kv7.2 channels, the G1S/A variants caused a drastic enhancement in maximal current density consistent with a GoF in vitro phenotype. The appearance of a tonic voltage-independent component (I_{INST}), together with a marked hyperpolarization in activation gating and a significant reduction in channel deactivation rate of the voltage-dependent current component (I_{VDEP}), seems to account for this enhancement. No differences in K^+ selectivity and pharmacological sensitivity to pore blockers such as TEA and Ba^{2+} were observed between I_{INST} and I_{VDEP} , suggesting that both components are carried via the same permeation pathway, i.e., the central ion pore.

To provide mechanistic insight into the molecular basis for this GoF effect, nonstationary noise analysis was used to estimate N , i , and P_o (20). Although channels with rather low P_o such as Kv7.5 and Kv7.2 (0.22 and 0.17, respectively) (21) do not unambiguously show signs of saturation in their variance/mean current plots, thereby leading to possible uncertainties in P_o estimates, simulation experiments have shown that these parameters can be more reliably calculated if a sufficient number of sweeps are analyzed and/or constraints are imposed on initial estimates of i (23). The observation that P_o values did not differ when estimated with constrained or unconstrained fits of nonstationary noise analysis data suggests that the G1S variant caused a 2.5–/3-fold increase in maximal P_o of both Kv7.5 and Kv7.2 channels, without major effects on the number of functional channels or their single-channel current amplitude. Notably, the P_o and i estimates herein obtained for both wild-type Kv7.5 and Kv7.2 channels are highly consistent with those achieved by single-channel recordings (*SI Appendix, Table S1*); moreover, a recent study using variance analysis reported a maximal P_o value for Kv7.2 channels (0.27) identical to the one herein estimated (44).

In all Kv7 subunits, the distal portion of the S_6 domain plays an important role in channel gating. Indeed, within this region, the PAG motif (corresponding to the conserved PXP motif of other Kv channels; Fig. 1*B*) is considered as the gating hinge for pore opening (45, 46). Cryogenic electron microscopy (Cryo-EM) studies have also revealed that in Kv7.1 channels, the signature GSG motif past the PXP motif forms the narrowest restriction along the ion conduction pathway (47). Our results reveal that in both Kv7.2 and Kv7.5 channels, the replacement of G1 with either a hydrophilic S or a hydrophobic A increased channel function by enhancing pore opening probability, whereas large, permanently charged residues (either the positive R or the negative E) fully impeded channel function and caused LoF effects. Our homology model of Kv7.5 revealed that the side chains of large and/or charged residues (R and E) introduced at position G1 occupy the central region of the activated/open pore configuration, thereby impeding ion flux (*SI Appendix, Fig. S2*);

instead, replacement of the helix-destabilizing G1 with an S residue likely reduces the flexibility of this region, thereby favoring the pore open state configuration. Notably, also in Kv7.1 channels, G1A replacement caused a relative stabilization of the open state over the closed state (13), thus confirming the common functional role played by G1 in all Kv7 subunits.

The anionic phospholipid PIP_2 acts as a critical gating modulator of Kv7 channels (26); by this mechanism, fluctuations in brain PIP_2 availability would translate into neuronal excitability changes (48). Increased PIP_2 availability facilitates both voltage-dependent and voltage-independent transitions toward the open state. Our data suggest that, at least for Kv7.2 channels, the GoF effects introduced by the G1S variant are PIP_2 -independent as mutant channels are resistant to inhibition or potentiation when PIP_2 levels are decreased or increased, respectively. Structural studies in Kv7.1 channels have recently shown that PIP_2 binding causes the C-terminal half of S_6 to bend at the conserved PAG motif, triggering a significant dilatation of the inner gate of the cytoplasmic pore; in particular, the GSG region expands from about 1 to >3.5 Å (49). Similar opening mechanisms through bending of S_6 have also been observed in other channels (50–52). We therefore hypothesize that the G1S/A substitutions prompt structural transitions resembling those triggered by PIP_2 binding, namely, an expansion of the S_6 helices which locks Kv7 channels in a constitutively open state. Consistent with this hypothesis is the ability of PIP_2 to prompt changes in channel function similar to those triggered by the G1S mutations, namely, a hyperpolarizing shift in activation $V_{1/2}$ and an increased maximal P_o at depolarized voltages (24, 26, 27).

Conclusions

Assessment of the functional consequences of rare variants in ion channel genes, besides revealing pathogenic mechanisms and genotype–phenotype correlations, is critical for diagnostic evaluation, prognostic predictions, and tailored therapeutic management of patients with a wide spectrum of neurological disorders. In this work, we identified two GoF variants in the pore region of Kv7.5 in two patients with ID \pm epilepsy, thereby further highlighting the role of Kv7.5 channel in neurodevelopmental disorders. Functional analysis revealed that the GoF effects were due to an increased opening probability as the disease pathogenic mechanism, thus providing structure–function insights into Kv7 channel gating and regulation.

Materials and Methods

Patient Recruitment and Genetic Analyses. The two patients were recruited in the Pediatric Neurology and Genetics Departments of the University Hospitals of Lyon and Lille, respectively. The parents gave informed consent for the genetic study and the publication, according to the French Bioethics law. The study was approved by the Ethics and Scientific Committees of the Lyon and Lille University Hospitals (no. 542, Gene Panel for Monogenic Epilepsies). Genetic diagnosis was performed using next-generation sequencing (exome sequencing for patient 1 and gene panel for patient 2), as described (53).

Mutagenesis and Heterologous Expression of *KCNQ2* and *KCNQ5* cDNAs. Mutations were engineered in human *KCNQ5* cloned into pcDNA3.1zeo and human *KCNQ2* cDNA cloned into pcDNA3 by QuikChange site directed mutagenesis (Agilent Technologies), as described (18). Channel subunits were expressed in CHO or HEK293 cells by transient transfection. CHO or HEK293 cells were grown in 100 mm plastic Petri dishes in Dulbecco's Modified Eagle Medium (DMEM) containing 10% fetal bovine serum (FBS), penicillin (50 U/mL), and streptomycin (50 μ g/mL) in a humidified atmosphere at 37 °C with 5% CO_2 . For

electrophysiological experiments, cells were seeded on glass coverslips in 40-mm dishes and transfected on the next day with the appropriate cDNAs using Lipofectamine 2000 (Invitrogen) according to the manufacturer's protocol. A plasmid encoding enhanced green fluorescent protein (Clontech) was used as transfection marker; total cDNA in the transfection mixture was kept constant at 4 μ g.

Whole-Cell Electrophysiology and Nonstationary Noise Analysis. Currents from CHO or HEK293 cells were recorded at room temperature (20 to 22 °C) 1 to 3 d after transfection, using commercially available amplifiers (Axopatch 200, Molecular Devices) and the whole-cell configuration of the patch-clamp technique, with glass micropipettes of 1 to 5 M Ω resistance. The extracellular solution contained (in mM) the following: 138 NaCl, 5.4 KCl, 2 CaCl₂, 1 MgCl₂, 10 glucose, and 10 Hepes, pH 7.4, with NaOH. The pipette (intracellular) solution contained (in mM) the following: 140 KCl, 2 MgCl₂, 10 ethylene glycol-bis-(beta-aminoethylether)-N,N,N',N'-tetraacetic acid (EGTA), 10 Hepes, 5 Mg-ATP, pH 7.3–7.4 with potassium hydroxide (KOH). The pCLAMP software (version 10.0.2) was used for data acquisition and analysis. Currents were corrected off-line for linear capacitance and leakage currents using standard subtraction routines (Clampfit module of pCLAMP 10). Current densities (expressed in pA/pF) were calculated as peak K⁺ currents at 0 mV divided by cell capacitance. Data were acquired at 0.5 to 2 kHz and filtered at 1 to 5 kHz with the four-pole low-pass Bessel filter of the amplifier. No corrections were made for liquid junction potentials. To generate conductance–voltage curves, the cells were held at –80 mV, then depolarized for 1.5 s from –80 to +20/40 mV in 10-mV increments, followed by an isopotential pulse at 0 mV of 300 ms duration; the current values recorded at the beginning of the 0 mV pulse were measured, normalized, and expressed as a function of the preceding voltages. The data were then fit to a Boltzmann distribution of the following form:

$$y = \max/[1 + \exp(V_{1/2} - V)/k], \quad [1]$$

where V is the test potential, $V_{1/2}$ is the half-activation potential, and k is the slope factor. In the experiments with 100 mM TEA_e shown in Fig. 1G, the NaCl concentration in the extracellular solution was reduced from 138 to 38 mM to preserve osmolarity (290 to 300 mOsm/L). With each blocker, fractional inhibition of I_{INST} was calculated as $1 - (A_2/A_1) \times 100$, whereas that of I_{DEP} was calculated as $1 - (B_2 - A_2/B_1 - A_1) \times 100$. Experimental procedures followed in the experiments with DrVSP and PIP5K, whose results are shown in Fig. 4, were carried out as previously described (27).

For noise analysis, 100 pulses of 500-ms duration were applied to a test voltage of 20 mV from the holding potential of –80 mV at 1 Hz frequency. Currents were low-pass filtered at 10 kHz and sampled at 100 kHz. Nonstationary noise analysis was performed according to the method of Heinemann and Conti (20). Variance was obtained by averaging the squared difference of consecutive records after appropriate scaling. Baseline variance was subtracted, and the variance–mean plot was fitted by the equation

$$\sigma^2 = i \langle I \rangle - \frac{\langle I \rangle^2}{N}, \quad [2]$$

where σ^2 is the variance and $\langle I \rangle$ is the mean current and with the free parameters i (single-channel current) and N (number of channels), without weighting factors by their SE. The maximal open probability was calculated as $P_{\text{max}} = \langle I \rangle_{\text{peak}} / (Ni)$. The GePulse program and the Ana program (<http://users.ge.ibf.cnr.it/pusch/programs-mik.htm>) were used, respectively, for data acquisition and analysis.

Cell-Surface Biotinylation and Western Blot. Isolation of plasma membrane proteins from CHO cells was performed via biotinylation of cell-surface proteins (32). Briefly, cells were incubated with Sulfo-NHS-LC-Biotin (0.5 mg/mL; Thermo Fisher), a cell membrane-impermeable reagent, for 20 min at 4 °C; the reaction was quenched with 0.1 M glycine in PBS, pH 8.0 (three washes, 20 min each). Subsequently, cells were lysed, and protein lysate was incubated with

streptavidin beads (Thermo Fisher) to isolate biotinylated proteins. Samples were separated by sodium dodecyl sulphate–polyacrylamide gel electrophoresis (SDS-PAGE) and transferred onto a polyvinylidene fluoride membrane (Merck). Membrane strips were incubated overnight at 4 °C with a rabbit polyclonal anti-Kv7.5 (Merck, dilution 1:2,000), and reactive bands were detected by enhanced chemiluminescence (ECL, Thermo Fisher) using autoradiography films. An anti- α -tubulin antibody (Merck, dilution 1:5,000) was used to check for equal protein loading and to assess the purity of the plasma membrane preparation. Optical densities (OD) of Kv7.5 and α -tubulin-reactive bands were calculated using Quantity One analysis software (Bio-Rad); OD of Kv7.5 bands were divided by those of α -tubulin-reactive bands, used as internal controls. Levels of plasma membrane Kv7.5 protein were normalized to total Kv7.5 protein input.

Structural Modeling. A three-dimensional model of the Kv7.5 subunit was generated by using as template the coordinates of human Kv7.1 in the activated/open state (Protein Data Bank [PDB] ID 5VM5) obtained in molecular dynamics simulations (54) of the recently published cryo-EM structure of *Xenopus laevis* KCNQ1 (48). Modeling of the S₅–S₆ pore domain was performed with the SWISS-MODEL software (<http://swissmodel.expasy.org>). The models were optimized through all-atom energy minimization by using the Groningen Molecular Simulation (GROMOS96) implementation of Swiss-PDBViewer and analyzed using both the DeepView module of Swiss-PDBViewer (version 4.0.1; <https://spdbv.vital-it.ch/>) and PyMOL (<https://pymol.org/2/>).

Statistics. Data are expressed as the mean \pm SE (SEM) of cells recorded in at least three independent experimental sessions. If not otherwise stated, statistical significance was assessed using the Student's t test, and the threshold P value for statistical significance levels was set at $P < 0.05$.

Data Availability. All study data are included in the article and/or *SI Appendix*.

ACKNOWLEDGMENTS. We thank Professors Mark S. Shapiro (Department of Cellular and Integrative Physiology, University of Texas Health Science Center, San Antonio, Texas), Thomas Jentsch (Department of Physiology and Pathology of Ion Transport, Leibniz-Institut für Molekulare Pharmakologie, Berlin, Germany), Alvaro Villarreal (University of the Basque Country, Leioa, Spain), and Yasushi Okamura (Osaka University, Suita, Osaka, Japan) for sharing hKCNQ5, hKCNQ2, PIP(4)5K, and Dr-VSP-IRES-GFP cDNAs, respectively. M.T. received funding from the Italian Ministry for University and Research (MIUR) (Progetti di Ricerca di Interesse Nazionale [PRIN] 2017ALCR7C), the Italian Ministry of Health (Project RF-2019-12370491), the European Commission H2020 (Up-scaling the global uNlvoac identification Of Medicines [UNICOM] 875299), the European Joint Programme on Rare Diseases (EJP RD) 2020 (TreatKCNQ). F.M. received funding from MIUR (PRIN 2017YH3SXX). M.P. received funding from the Fondazione Associazione Italiana per la Ricerca sul Cancro (AIRC; grant IG 21558) and from MIUR (PRIN 20174TB8KW). M.V.S. received funding from the Italian Ministry of Health (Project GR-2016-02363337) and MIUR (PRIN 2017ALCR7C).

Author affiliations: ^aDepartment of Neuroscience, University of Naples "Federico II", 80131 Naples, Italy; ^bDepartment of Medical Genetics, Lyon University Hospital, 69677 Lyon, France; ^cPediatric Neurology, Lyon University Hospital, Claude Bernard Lyon 1 University, 69677 Lyon, France; ^dEquipe d'Accueil 7364, Maladies Rares du Développement Embryonnaire et du Métabolisme, Institut de Génétique Médicale, Centre Hospitalier Universitaire de Lille, Université de Lille, F-59000 Lille, France; ^eClinique de Génétique–Guy Fontaine, Centre Hospitalier Universitaire de Lille, F-59000 Lille, France; ^fDepartment of Pediatrics, Hôpital Nord-Ouest, Villefranche-sur-Saône, 69400 France; ^gDepartment of Medicine and Health Science, University of Molise, 86100 Campobasso, Italy; ^hDepartment of Science and Technology, University of Sannio, Benevento, 82100 Italy; and ⁱInstitute of Biophysics, Italian National Research Council, 16149 Genova, Italy

1. H. Kearney, S. Byrne, G. L. Cavalleri, N. Delanty, Tackling epilepsy with high-definition precision medicine: A review. *JAMA Neurol.* **76**, 1109–1116 (2019).
2. N. Dirx, F. Miceli, M. Tagliatalata, S. Weckhuysen, The role of Kv7.2 in neurodevelopment: Insights and gaps in our understanding. *Front. Physiol.* **11**, 570588 (2020).
3. F. Jones, N. Gamper, H. Gao, "Kv7 channels and excitability disorders" in *Handbook of Experimental Pharmacology*, N. Gamper, K. Wang, Eds. (Springer, 2021), pp. 185–230.
4. C. Lerche *et al.*, Molecular cloning and functional expression of KCNQ5, a potassium channel subunit that may contribute to neuronal M-current diversity. *J. Biol. Chem.* **275**, 22395–22400 (2000).

5. B. C. Schroeder, M. Hechenberger, F. Weinreich, C. Kubisch, T. J. Jentsch, KCNQ5, a novel potassium channel broadly expressed in brain, mediates M-type currents. *J. Biol. Chem.* **275**, 24089–24095 (2000).
6. A. Lehman *et al.*, CAUSES Study; EPGEN Study, Loss-of-function and gain-of-function mutations in KCNQ5 cause intellectual disability or epileptic encephalopathy. *Am. J. Hum. Genet.* **101**, 65–74 (2017).
7. G. Rosti *et al.*, Intragenic duplication of KCNQ5 gene results in aberrant splicing leading to a premature termination codon in a patient with intellectual disability. *Eur. J. Med. Genet.* **62**, 103555 (2019).

8. A. V. Zzingounis *et al.*, The KCNQ5 potassium channel mediates a component of the afterhyperpolarization current in mouse hippocampus. *Proc. Natl. Acad. Sci. U.S.A.* **107**, 10232–10237 (2010).
9. P. Fidzinski *et al.*, KCNQ5 K(+) channels control hippocampal synaptic inhibition and fast network oscillations. *Nat. Commun.* **6**, 6254 (2015).
10. F. Miceli *et al.*, Pharmacological targeting of neuronal Kv7.2/3 channels: A focus on chemotypes and receptor sites. *Curr. Med. Chem.* **25**, 2637–2660 (2018).
11. H. Soh, R. Pant, J. J. LoTurco, A. V. Zzingounis, Conditional deletions of epilepsy-associated KCNQ2 and KCNQ3 channels from cerebral cortex cause differential effects on neuronal excitability. *J. Neurosci.* **34**, 5311–5321 (2014).
12. N. Gamper, J. D. Stockand, M. S. Shapiro, Subunit-specific modulation of KCNQ potassium channels by Src tyrosine kinase. *J. Neurosci.* **23**, 84–95 (2003).
13. I. R. Boulet, A. J. Labro, A. L. Raes, D. J. Snyders, Role of the S6 C-terminus in KCNQ1 channel gating. *J. Physiol.* **585**, 325–337 (2007).
14. M. Tagliatalata *et al.*, Patterns of internal and external tetraethylammonium block in four homologous K⁺ channels. *Mol. Pharmacol.* **40**, 299–307 (1991).
15. M. Tagliatalata, J. A. Drewe, A. M. Brown, Barium blockade of a clonal potassium channel and its regulation by a critical pore residue. *Mol. Pharmacol.* **44**, 180–190 (1993).
16. H. E. Olson *et al.*, Genetics and genotype-phenotype correlations in early onset epileptic encephalopathy with burst suppression. *Ann. Neurol.* **81**, 419–429 (2017).
17. C. Gomis-Pérez *et al.*, Homomeric Kv7.2 current suppression is a common feature in KCNQ2 epileptic encephalopathy. *Epilepsia* **60**, 139–148 (2019).
18. F. Miceli *et al.*, Genotype-phenotype correlations in neonatal epilepsies caused by mutations in the voltage sensor of Kv7.2 potassium channel subunits. *Proc. Natl. Acad. Sci. U.S.A.* **110**, 4386–4391 (2013).
19. G. Orhan *et al.*, Dominant-negative effects of KCNQ2 mutations are associated with epileptic encephalopathy. *Ann. Neurol.* **75**, 382–394 (2014).
20. S. H. Heinemann, F. Conti, Nonstationary noise analysis and application to patch clamp recordings. *Methods Enzymol.* **207**, 131–148 (1992).
21. Y. Li, N. Gamper, M. S. Shapiro, Single-channel analysis of KCNQ K⁺ channels reveals the mechanism of augmentation by a cysteine-modifying reagent. *J. Neurosci.* **24**, 5079–5090 (2004).
22. D. Sigg, E. Stefani, F. Bezanilla, Gating current noise produced by elementary transitions in Shaker potassium channels. *Science* **264**, 578–582 (1994).
23. C. J. Lingle, Empirical considerations regarding the use of ensemble-variance analysis of macroscopic currents. *J. Neurosci. Methods* **158**, 121–132 (2006).
24. R. Y. Kim, S. A. Pless, H. T. Kurata, PIP2 mediates functional coupling and pharmacology of neuronal KCNQ channels. *Proc. Natl. Acad. Sci. U.S.A.* **114**, E9702–E9711 (2017).
25. M. I. Hossain *et al.*, Enzyme domain affects the movement of the voltage sensor in ascidian and zebrafish voltage-sensing phosphatases. *J. Biol. Chem.* **283**, 18248–18259 (2008).
26. B. H. Falkenburger, J. B. Jensen, B. Hille, Kinetics of PIP2 metabolism and KCNQ2/3 channel regulation studied with a voltage-sensitive phosphatase in living cells. *J. Gen. Physiol.* **135**, 99–114 (2010).
27. M. V. Soldovieri *et al.*, Early-onset epileptic encephalopathy caused by a reduced sensitivity of Kv7.2 potassium channels to phosphatidylinositol 4,5-bisphosphate. *Sci. Rep.* **6**, 38167 (2016).
28. P. Nappi *et al.*, Epileptic channelopathies caused by neuronal Kv7 (KCNQ) channel dysfunction. *Pflugers Arch.* **472**, 881–898 (2020).
29. J. Kaplanis *et al.*, Deciphering Developmental Disorders Study, Evidence for 28 genetic disorders discovered by combining healthcare and research data. *Nature* **586**, 757–762 (2020).
30. S. H. Lelieveld *et al.*, Meta-analysis of 2,104 trios provides support for 10 new genes for intellectual disability. *Nat. Neurosci.* **19**, 1194–1196 (2016).
31. J. D. Symonds *et al.*, Incidence and phenotypes of childhood-onset genetic epilepsies: A prospective population-based national cohort. *Brain* **142**, 2303–2318 (2019).
32. F. Miceli *et al.*, Early-onset epileptic encephalopathy caused by gain-of-function mutations in the voltage sensor of Kv7.2 and Kv7.3 potassium channel subunits. *J. Neurosci.* **35**, 3782–3793 (2015).
33. J. J. Millichap *et al.*, Infantile spasms and encephalopathy without preceding neonatal seizures caused by KCNQ2 R198Q, a gain-of-function variant. *Epilepsia* **58**, e10–e15 (2017).
34. S. B. Mulkey *et al.*, Neonatal nonepileptic myoclonus is a prominent clinical feature of KCNQ2 gain-of-function variants R201C and R201H. *Epilepsia* **58**, 436–445 (2017).
35. T. T. Sands *et al.*, Autism and developmental disability caused by KCNQ3 gain-of-function variants. *Ann. Neurol.* **86**, 181–192 (2019).
36. M. Gilling *et al.*, Dysfunction of the heteromeric Kv7.3/Kv7.5 potassium channel is associated with autism spectrum disorders. *Front. Genet.* **4**, 54 (2013).
37. H. S. Wang *et al.*, KCNQ2 and KCNQ3 potassium channel subunits: Molecular correlates of the M-channel. *Science* **282**, 1890–1893 (1998).
38. E. Yus-Nájera *et al.*, Localization of KCNQ5 in the normal and epileptic human temporal neocortex and hippocampal formation. *Neuroscience* **120**, 353–364 (2003).
39. H. Huang, L. O. Trussell, KCNQ5 channels control resting properties and release probability of a synapse. *Nat. Neurosci.* **14**, 840–847 (2011).
40. G. Spitzmaul *et al.*, Vestibular role of KCNQ4 and KCNQ5 K⁺ channels revealed by mouse models. *J. Biol. Chem.* **288**, 9334–9344 (2013).
41. G. Trompoukis, P. Rigas, L. J. Leontiadis, C. Papatheodoropoulos, I_h, GIRK, and KCNQ/Kv7 channels differentially modulate sharp wave-ripples in the dorsal and ventral hippocampus. *Mol. Cell. Neurosci.* **107**, 103531 (2020).
42. G. Buzsáki, Hippocampal sharp wave-ripple: A cognitive biomarker for episodic memory and planning. *Hippocampus* **25**, 1073–1188 (2015).
43. Z. Niday, A. V. Zzingounis, Potassium channel gain of function in epilepsy: An unresolved paradox. *Neuroscientist* **24**, 368–380 (2018).
44. X. Li *et al.*, Molecular basis for ligand activation of the human KCNQ2 channel. *Cell Res.* **31**, 52–61 (2021).
45. Y. Jiang *et al.*, The open pore conformation of potassium channels. *Nature* **417**, 523–526 (2002).
46. S. B. Long, E. B. Campbell, R. Mackinnon, Crystal structure of a mammalian voltage-dependent Shaker family K⁺ channel. *Science* **309**, 897–903 (2005).
47. J. Sun, R. MacKinnon, Cryo-EM structure of a KCNQ1/CaM complex reveals insights into congenital long QT syndrome. *Cell* **169**, 1042–1050.e9 (2017).
48. K. S. Kim, K. M. Duignan, J. M. Hawryluk, H. Soh, A. V. Zzingounis, The voltage activation of cortical KCNQ channels depends on global PIP2 levels. *Biophys. J.* **110**, 1089–1098 (2016).
49. J. Sun, R. MacKinnon, Structural basis of human KCNQ1 modulation and gating. *Cell* **180**, 340–347.e9 (2020).
50. R. K. Hite, R. MacKinnon, Structural titration of Slo2.2, a Na⁺-dependent K⁺ channel. *Cell* **168**, 390–399.e11 (2017).
51. R. K. Hite, X. Tao, R. MacKinnon, Structural basis for gating the high-conductance Ca²⁺-activated K⁺ channel. *Nature* **541**, 52–57 (2017).
52. C. H. Lee, R. MacKinnon, Activation mechanism of a human SK-calmodulin channel complex elucidated by cryo-EM structures. *Science* **360**, 508–513 (2018).
53. G. Rudolf *et al.*, Exome sequencing in 57 patients with self-limited focal epilepsies of childhood with typical or atypical presentations suggests novel candidate genes. *Eur. J. Paediatr. Neurol.* **27**, 104–110 (2020).
54. G. Kuenze *et al.*, Upgraded molecular models of the human KCNQ1 potassium channel. *PLoS One* **14**, e0220415 (2019).